THIS MANUSCRIPT HAS BEEN SUBMITTED TO THE ANNALS OF GLACIOLOGY AND HAS NOT BEEN PEER-REVIEWED.

Topographic control on ice anisotropy in Antarctic ice rises inferred from phase-sensitive radar

Journal:	*Annals of Glaciology*
Manuscript ID	AOG-99-0587
Manuscript Type:	Article
Date Submitted by the Author:	26-Aug-2026
Complete List of Authors:	Gillain, Marie-Axelle; Université Libre de Bruxelles, Laboratoire de Glaciologie Martin, Carlos; British Antarctic Survey, Ice Dynamics and Paleoclimate Pattyn, Frank; Universite Libre Bruxelles Faculte des Sciences, Laboratoire de Glaciologie
Keywords:	Anisotropic ice, Antarctic glaciology, Ice rheology, Ice rise, Radio-echo sounding
Abstract:	The Raymond effect within ice rises and underneath ice divides of ice sheets arises from the non-linear rheology of the ice and steady-flow conditions. The resulting Raymond arches seen in radargrams have been associated with crystal orientation fabric (COF) that produces ice optical anisotropy, detectable with radar. We use data collected with a phase-sensitive radar across two ice rises, Hammarryggen and Lokeryggen, both located in Dronning Maud Land, East Antarctica. Despite their proximity, Raymond arches are observed at Hammarryggen but are absent at Lokeryggen. The absence of Raymond arches does not necessarily arise from non-steady conditions close to the bed, but may be controlled by the more complex bedrock topography that reduces ice anisotropy and resulting ice stiffening.

Topographic control on ice anisotropy in Antarctic ice rises inferred from phase-sensitive radar

Marie-Axelle GILLAIN[1]*, Carlos MARTÍN[2], Frank PATTYN[1]

[1]*Laboratoire de Glaciologie, Université libre de Bruxelles, Brussels, Belgium*

[2]*British Antarctic Survey, Natural Environment Research Council, Cambridge, UK*

Correspondence: Marie-Axelle Gillain <marie-axelle.gillain@ulb.be>

ABSTRACT. The Raymond effect within ice rises and underneath ice divides of ice sheets arises from the non-linear rheology of the ice and steady-flow conditions. The resulting Raymond arches seen in radargrams have been associated with crystal orientation fabric (COF) that produces ice optical anisotropy, detectable with radar. We use data collected with a phase-sensitive radar across two ice rises, Hammarryggen and Lokeryggen, both located in Dronning Maud Land, East Antarctica. Despite their proximity, Raymond arches are observed at Hammarryggen but are absent at Lokeryggen. The absence of Raymond arches does not necessarily arise from non-steady conditions close to the bed, but may be controlled by the more complex bedrock topography that reduces ice anisotropy and resulting ice stiffening.

INTRODUCTION

Ice rises are locally grounded features in Antarctic ice shelves and play a key role in buttressing ice discharge from the Antarctic ice sheet (Matsuoka and others, 2015). Since ice rises are local flow features, each with a distinct ice divide, they also preserve records of past ice-flow dynamics within their internal structure. For instance, beneath ice rise divides, ice stiffens due to its non-linear rheology and steady-flow conditions, resulting in the so-called Raymond effect (Raymond, 1983; Martín and others, 2009a). This mechanism forms layered arches, known as Raymond arches, and their formation and amplitude are controlled by both

*Present address: Laboratoire de Glaciologie, Université libre de Bruxelles, Brussels, Belgium.

the mechanical properties of the ice and the stress gradient between the divide and the flanks of the ice rise (Pettit and Waddington, 2003). Given the strong influence of ice anisotropy on these mechanical features, Raymond arches provide valuable insight into the processes governing ice flow dynamics and divide stability (Raymond, 1983; Martín and others, 2009a; Ershadi and others, 2022).

Ice anisotropy develops differently across ice rises, and is mainly controlled by local stress regimes, which influence the crystalline structure of the ice (Matsuoka and others, 2015; Hills and others, 2025a,b). The ice divide flow regime is dominated by vertical compression due to accumulation (Weikusat and others, 2017), driving crystal alignment along the principal axis of compression and resulting in stiffer ice fabric and increased mechanical anisotropy (Alley, 1992; Passchier, 1997). On the ice-rise flanks, larger deviatoric stresses lead to horizontal stretching, resulting in a redistribution of c-axes within the plane of extension (Martín and others, 2009a, 2015; Brisbourne and others, 2019). The resulting crystal organization, known as the crystal orientation fabric (COF), reflects the internal stress history of the ice rise. The COF therefore constitutes both an archive of past ice flow regimes and a driver of current ones (Alley, 1992).

Exploiting the fabric record, however, requires robust characterization of COF across ice rises (Alley, 1992; Martín and others, 2009a; Ershadi and others, 2022). Ice fabric was historically accessed using ice cores, which long represented the only source of COF information despite several major drawbacks (e.g., important logistics, time-consuming processing, and potential crystal rotation within core samples; Ershadi and others, 2022). Innovative methods, such as seismic measurements, sonic logging of boreholes and phase-sensitive radars now enable COF characterization with lighter logistics (Ershadi and others, 2022). In particular, depth profiles of COF can be reconstructed from quad-polarimetric phase-sensitive Radio Echo Sounding (pRES) and inverse modelling, an approach that has gained increasing attention in recent years (Fujita and others, 2006; Brisbourne and others, 2019; Jordan and others, 2019; Ershadi and others, 2022; Zeising and others, 2023; Ershadi and others, 2025; Henry and others, 2025; Hills and others, 2025a,b). Inverse modelling relies on variations with depth in the power and phase of the backscattered radar signal, which arise from changes in the crystal arrangement responsible for dielectric anisotropy (Brisbourne and others, 2019). Combined, pRES measurements and inverse modelling provide valuable constraints on ice rheology and ice-flow dynamics (Kingslake and others, 2014). In this framework, ice cores can now help to calibrate and validate inversion results (Young and others, 2021; Ershadi and others, 2022; Zeising and others, 2023; Ershadi and others, 2025).

Here, we infer COF along two transects crossing the summits of two nearby promontory ice rises in

Dronning Maud Land, Antarctica, i.e., Hammarryggen and Lokeryggen Ice Rises (Figure 1). We exploit the mathematical and optical relationships between dielectric anisotropy and the COF (Fujita and others, 2006; Ershadi and others, 2022) using quad-polarimetric pRES point measurements and inverse modelling. While the Hammarryggen fabric and dynamics have already been described in Ershadi and others, 2025 and Koch and others, 2024, recent measurements on the nearby Lokeryggen ice rise now allow for an in-depth comparison of COF evolution. Finally, we discuss the differences between both sites in terms of anisotropy and discuss the potential role of bedrock topography in their fabric signatures.

METHODS

Study area

Hammarryggen and Lokeryggen are two promontory ice rises located in Dronning Maud Land, East Antarctica, each connected to the ice sheet through a saddle. Quad-polarimetric data were collected across the centre of both ice rises during the field seasons of 2018-2019 and 2020-2021 (Figure 1; Pattyn and others, 2023; Gillain and others, 2026). Hammarryggen is a triple junction ice rise, where 15 pRES measurements were acquired along a 5 km transect (∼ 70.5°S, 21.8°E) (Figure 1b). Lokeryggen is located ∼75 kilometres to the east, where 21 measurements were collected along a 6 km transect (∼ 70.5°S, 24.1°E) (Figure 1d). For both transects, the measurements were spaced more closely near the divide (100 m apart) than on the flanks (500 m apart). The summit of Hammarryggen reaches 367 m above sea level with a corresponding ice thickness of 550 m (Ershadi and others, 2025). During the 2018-2019 field season, an ice core was drilled at the ice divide (Pattyn and others, 2023; Ershadi and others, 2025). The Lokeryggen summit reaches 350 m above sea level with a corresponding ice thickness of 430 m.

Phase-sensitive radar data collection

The phase-sensitive radar system (Nicholls and others, 2015) uses a Frequency Modulated Continuous Wave (FMCW) approach, emitting a chirp that propagates through the ice column via the transmitting antenna and is recorded by a receiving antenna. The transmitted signal varies across a frequency range of 200 to 400 MHz, corresponding to a central frequency of 300 MHz (Nicholls and others, 2015; Hills and others, 2025b). By comparing the transmitted and backscattered signals, the system determines variations in amplitude and phase, allowing the detection of internal reflectors. As the radar wave propagates through the ice, the velocity of the signal is influenced by the dielectric properties of the medium. In a single crystal,

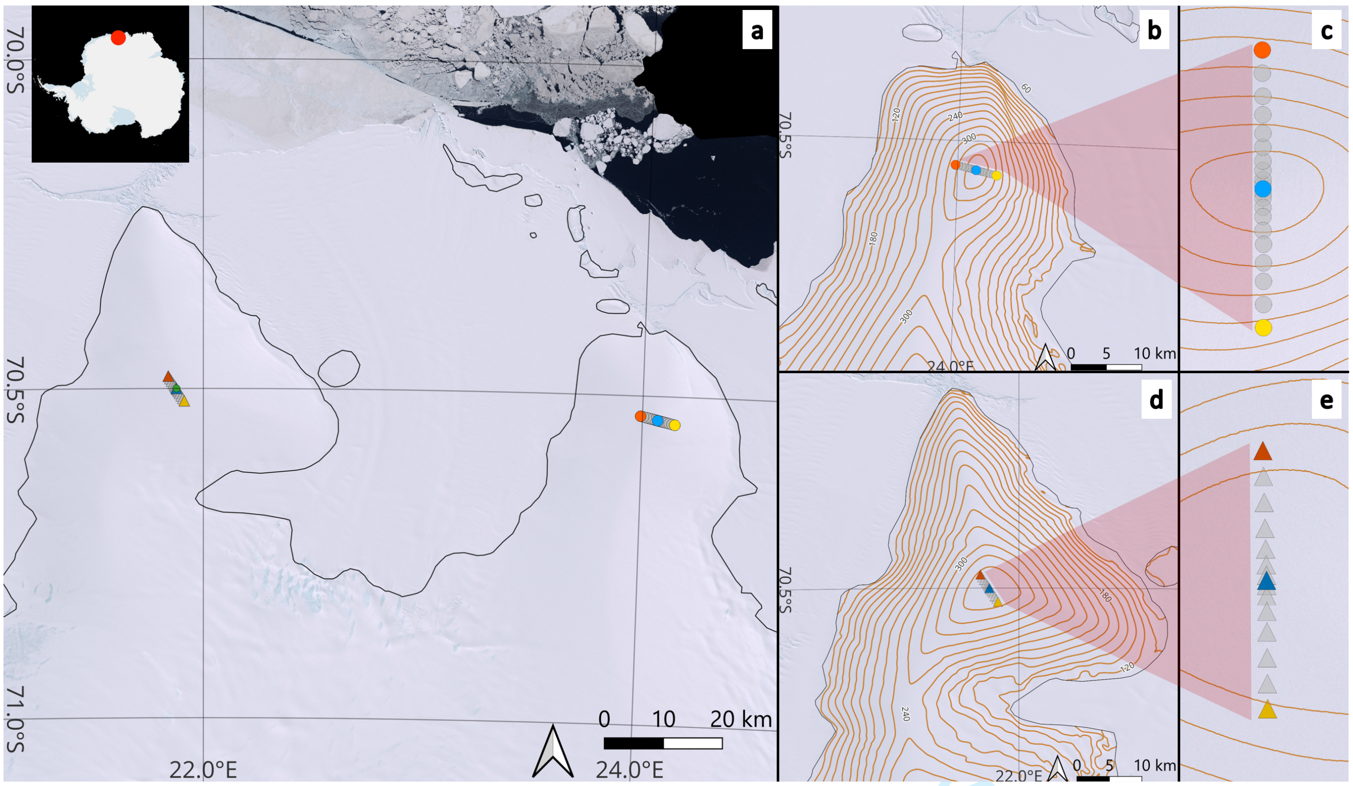

Fig. 1. Study area. (a) Location of Lokeryggen and Hammarryggen showing the ApRES survey transects. (b-e) Close-ups of Hammarryggen and Lokeryggen showing the ApRES measurement sites (triangular and circular dots) and the ice-core location (green dot). Background imagery from the Landsat Image Mosaic of Antarctica (LIMA) (Bindschadler and others, 2008). Maps were produced using QGIS (QGIS Development Team, 2026).

dielectric anisotropy arises from uniaxial birefringent properties, the dielectric permittivity along the c-axis being larger than that in the basal plane (Gerber and others, 2023). In polycrystalline ice, an effective dielectric permittivity emerges from the combined effects of density, acidity, and COF, which in turn affects radar signal propagation (Brisbourne and others, 2019). Depending on the crystal orientation relative to the radar signal, the returned signal varies, resulting in birefringence and anisotropic scattering observable in radargrams. In particular, the crystal orientation relative to the wave polarization leads to changes in the amplitude and phase of the backscattered signal, as a function of the antenna orientation (Brisbourne and others, 2019). This variability can be detected with millimetre precision, and fully captured using quad-polarimetric measurements (Sun and others, 2019; Ershadi and others, 2025).

To perform quad-polarimetric measurements, the two antennas are separated by 5 m. They are then rotated into four different polarization combinations: both vertically (VV), both horizontally (HH), vertical-horizontal (VH) and horizontal-vertical (HV). HH and VV consist of co-polarimetry, while HV and VH correspond to cross-polarimetry. Together, these four configurations constitute quad-polarimetry and allow for efficient reconstruction of the signal at any azimuthal orientation (Jordan and others, 2019; Young and others, 2021). These four polarimetric measurements are jointly processed through the Scattering or Sinclair matrix **S**, to derive the full azimuthal variation of both the phase difference and the power of the backscattered signal at each measurement site (Fujita and others, 2006; Young and others, 2021; Ershadi and others, 2022):

$$S = \begin{pmatrix} s_{hh} & s_{hv} \\ s_{vh} & s_{vv} \end{pmatrix}, \tag{1}$$

where s_{hh} and s_{vv} correspond to the intensity of the back-scattered signal in co-polarized configuration, and s_{hv} and s_{vh} correspond to the intensity of the back-scattered signal in cross-polarized configuration (Jordan and others, 2019). From these measurements, we reconstruct COF with depth using an inverse model. The model azimuthal reconstruction of the signal was validated against COF measurements from the EPICA Dronning Maud Land ice core, showing strong agreement (Ershadi and others, 2022).

Inverse model

The inverse model used for this study is fully described in Ershadi and others (2022), and is built on the forward model of Fujita and others (2006). The model quantifies horizontal anisotropy ($\Delta\lambda_H$) and the direction of the strongest horizontal eigenvector ($\vec{v}_2$) in polycrystalline ice, based on the relative magnitude of the dielectric permittivity tensor horizontal components ϵ'_x and ϵ'_y. Both are derived from the HH, HV and HHVV coherence phase, under the assumption that the vertical eigenvector is oriented vertically (Fujita and others, 2006; Ershadi and others, 2025). Following the recommendations on coherence magnitude from Jordan and others (2019), the inversion for Hammarryggen stops at 400 m, and for Lokeryggen at 350 m, covering around 70% of the ice column at the divide. Beyond these depths, the coherence between s_{hh} and s_{vv} becomes unreliable, introducing major uncertainties in the phase analysis (Ershadi and others, 2025).

Eigenvalues, eigenvectors and second order orientation tensor

To relate the statistical distribution of c-axes in space to radar signal propagation into the ice, Fujita and others (2006) considered the dielectric anisotropy of a single ice crystal, characterized by two permittivities, i.e., $\epsilon_\perp$ and $\epsilon_\parallel$, corresponding to the electric field oriented perpendicular and parallel to the crystal c-axis, respectively. The COF can be described by an orientation tensor corresponding to an ellipsoid locally describing the bulk fabric of the ice. The tensor is characterized by its eigenvalues $(\lambda_1, \lambda_2, \lambda_3)$ to quantify the relative concentration of c-axes along the tensor eigenvectors $(\vec{v}_1, \vec{v}_2, \vec{v}_3)$. The relation between the dielectric and the orientation tensor is given by (Fujita and others, 2006)

$$\epsilon' = \begin{pmatrix} \epsilon'_x & 0 & 0 \\ 0 & \epsilon'_y & 0 \\ 0 & 0 & \epsilon'_z \end{pmatrix} = \begin{pmatrix} \epsilon'_\perp + \lambda_1 \Delta\epsilon' & 0 & 0 \\ 0 & \epsilon'_\perp + \lambda_2 \Delta\epsilon' & 0 \\ 0 & 0 & \epsilon'_\perp + \lambda_3 \Delta\epsilon' \end{pmatrix}, \quad (2)$$

where $\Delta\epsilon' = \epsilon'_\perp - \epsilon'_\parallel$ is the magnitude of the anisotropic permittivity. As the propagating signal is sensitive to the dielectric anisotropy of the ice, represented by its dielectric tensor, birefringence and anisotropic scattering occur. Consequently, the signal is decomposed into two orthogonal components aligned with the two principal dielectric permittivity axes, controlled by COF and associated mechanical anisotropy (Jordan and others, 2019; Ershadi and others, 2022). The three eigenvalues in Eq. 2 sum to 1, i.e., $\lambda_1 + \lambda_2 + \lambda_3 = 1$, where $\lambda_1 < \lambda_2 < \lambda_3$. Their values are obtained from the orientation tensor. The

Table 1. Summary of fabric types and corresponding eigenvalues.

Fabric type	Eigenvalues
Isotropic	$\lambda_1 = \lambda_2 = \lambda_3$
Single maximum	$\lambda_3 > \lambda_2 \approx \lambda_1$
Girdle	$\lambda_3 \approx \lambda_2 > \lambda_1$

three eigenvectors represent a three-dimensional Cartesian coordinate system, in which $\vec{v}_3$ is assumed to point vertically (Ershadi and others, 2022). $\vec{v}_2$ and $\vec{v}_1$ are horizontal vectors and the direction of $\vec{v}_2$ is given by the georeferenced orientation of the horizontal anisotropy $\Delta\lambda_H$ (Fujita and others, 2006; Ershadi and others, 2022, 2025). Defining the orientation from the c-axis distribution, the eigenvalues and eigenvectors can be retrieved and used to determine the type of fabric, i.e., isotropic, single maximum (also referred to as cluster), or girdle.

In the absence of stress, ice is isotropic and the c-axes are uniformly distributed in all orientations, resulting in equal concentration along the three eigenvectors: $\lambda_1 \approx \lambda_2 \approx \lambda_3$. In the case of compaction, c-axes progressively orient themselves in the direction of the applied force, leading to a single maximum fabric (Alley, 1992). If a vertical stress is applied, c-axes are concentrated along $\vec{v}_3$, as represented by a greater value of λ_3: $\lambda_3 > \lambda_2 \approx \lambda_1$. The last case is a girdle fabric, defined by $\lambda_3 \approx \lambda_2 > \lambda_1$, so the c-axes are spread in the plane determined by $\vec{v}_3$ and $\vec{v}_2$ (Woodcock, 1977; Fujita and others, 2006). All fabric types are summarized in Table 1.

The inversion model follows a top-to-bottom approach by estimating the reflection ratio r and the horizontal anisotropy $\Delta\lambda_H$ to reconstruct the eigenvalues evolution with depth. The reflection ratio results from the division of the real part of the complex amplitude reflection coefficients Γ_x and Γ_y, parts of the Γ matrix. The reflection ratio r is calculated based on anisotropic scattering, caused by changes with depth in fabric, leading to differences in reflection and amplitude in the backscattered signal (Eq. 6 in Ershadi and others, 2022). $\Delta\lambda_H$ is proportional to the local phase gradient (Eqs. 10-11 in Ershadi and others, 2022), resulting from changes in COF and associated dielectric anisotropy. The birefringent nature of the ice affects the polarization of the backscattered signal. The signal is split into two orthogonal waves whose orientation depends on the relative orientation of the signal sent by the radar to the direction of the c-axes. Because of the dielectric anisotropy of the ice, the two components propagate at different velocities, inducing a phase shift (birefringence). As birefringence and anisotropic scattering can coexist, rotating the transmitting and receiving antennas enables the observation of the changes in phase and amplitude in the returned signal (Brisbourne and others, 2019). Using the inversion to estimate r and $\Delta\lambda_H$, it is then possible to reconstruct the three eigenvalues, assuming an isotropic material lying at the surface (Eqs. 20-24 in Ershadi and others, 2022).

Horizontal anisotropy, $\Delta\lambda_H$

Alternatively, $\Delta\lambda_H$ can be expressed directly from the eigenvalues as $\Delta\lambda_H = \lambda_2 - \lambda_1$, where λ_1 and λ_2 represent the concentration of c-axes along $\vec{v}_1$ and $\vec{v}_2$. A large value of $\Delta\lambda_H$ indicates c-axes strongly concentrated along $\vec{v}_2$, while a low value reflects a more distributed fabric between the two horizontal eigenvectors. Since the orientation of the receiving antenna is known, the direction of $\vec{v}_2$ can be determined and used as a proxy of the ice flow direction (Fujita and others, 2006; Ershadi and others, 2025).

Vertical anisotropy, $\Delta\lambda_V$

Similarly, the vertical anisotropy, defined by $\Delta\lambda_V = \lambda_3 - \lambda_2$, refers to the degree to which c-axes are concentrated along the vertical eigenvector $\vec{v}_3$ relative to the horizontal plane. Large values indicate a vertical clustered fabric, while low values reflect c-axes distributed between the vertical and horizontal planes (Ershadi and others, 2025).

Woodcock parameters, K and C

The Woodcock parameters are ratios of eigenvalues used to determine the type of fabric, K and the degree of fabric development or fabric intensity, C (Woodcock, 1977):

$$K = \frac{\ln(\lambda_3/\lambda_2)}{\ln(\lambda_2/\lambda_1)}\,, \tag{3}$$

$$C = \ln\left(\frac{\lambda_3}{\lambda_1}\right)\,. \tag{4}$$

Values of $\ln(K) > 0$ indicate a single maximum fabric, while $\ln(K) < 0$ indicates a girdle fabric (Henry and others, 2025). The fabric type is further complemented by its intensity. Values of $C > 2$ indicate a well-defined fabric, while lower values suggest a less pronounced one (Ershadi and others, 2025).

Vertical strain rate, $\dot{\varepsilon}_{zz}$

The vertical strain rate, $\dot{\varepsilon}_{zz}$, depicts the local rate of deformation. By repeating pRES measurements at the exact same locations across successive years, the downward displacement of internal reflectors relative to the bed can be tracked from phase changes in the backscattered signal, allowing the determination of averaged vertical velocities (Kingslake and others, 2014; Ershadi and others, 2025).

Values of the vertical strain rate are expected to be negative and of larger magnitude at the surface at the ice rise divide, where ice dynamics are dominated by compaction of snow and firn. Closer to the bed, they are expected to be smaller in magnitude due to cumulative vertical compression over time (Kingslake and others, 2014). Due to the Raymond effect, a local increase in the magnitude of the vertical strain rate can be observed at depth, reflecting the greater stiffness of the ice at the divide, which reduces vertical velocities.

RESULTS

Vertical clustering, λ_3

At both Hammarryggen and Lokeryggen, λ_3 increases with depth along the transect (Figure 2). At the divide, λ_3^{Ham} is consistently higher than λ_3^{Lok} throughout the ice column, indicating stronger vertical clustering at Hammarryggen. On the flanks, values of λ_3 are similar between the two ice rises. At Lokeryggen (Figure 2d), λ_3 increases more rapidly with depth on the west flank than at the centre and on the east flank, while the east flank shows the lowest values throughout the ice column, suggesting stronger fabric development on the west side of the ice rise.

The value of $\Delta\lambda_V$ increases with depth similarly at both ice rises (Figure S1). On the flanks, values are nearly identical between the two, though slightly higher at Hammarryggen, with larger values on the west flank than on the east flank. At the ice divide, however, $\Delta\lambda_V^{Ham}$ is significantly larger than $\Delta\lambda_V^{Lok}$ throughout the ice column, reflecting stronger vertical clustering at Hammarryggen. At Lokeryggen (Figure S1d), as for λ_3, the west flank shows larger values than at the centre and the east flank, indicating greater concentration of c-axes along the vertical axis.

Values of $\Delta\lambda_H$ vary similarly with depth at both ice rises, with good agreement from the surface to approximately 0.3 of the ice column (Figure S1). Both show a pronounced peak at around $0.35 - 0.4$ across the transect, and at 0.7 at the divide. However, $\Delta\lambda_H^{\text{Ham}}$ remains larger and shows more pronounced peaks

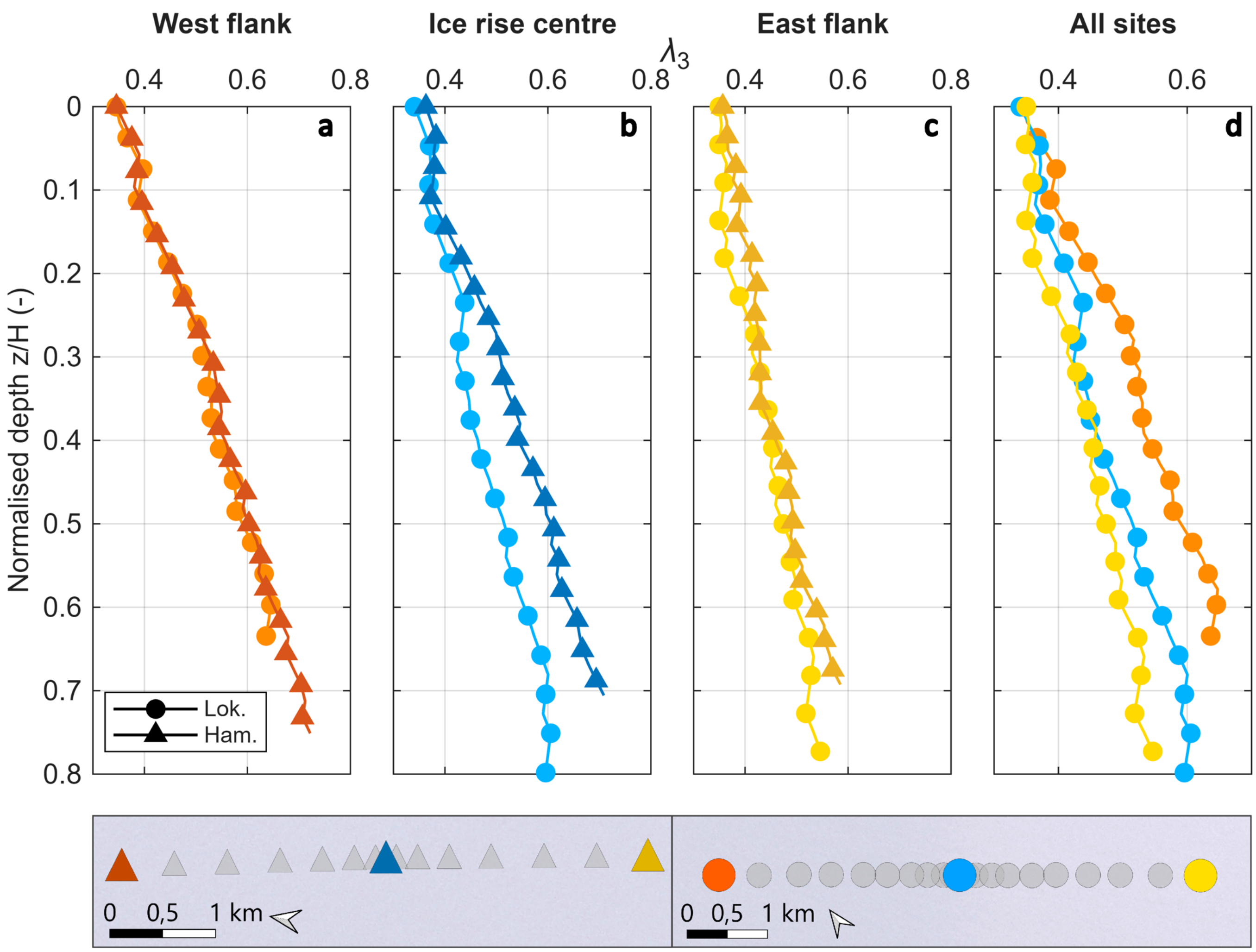

Fig. 2. Comparison of eigenvalues λ_3 with depth at the flanks and the centre of Lokeryggen and Hammarryggen. Panel d displays Lokeryggen λ_3 profiles.

than $\Delta\lambda_H^{\mathrm{Lok}}$ throughout the transect. These local maxima indicate local predominant horizontal c-axis alignment along the $\vec{v}_2$ direction, suggesting bands of lateral extension at the same depth in both ice rises (Ershadi and others, 2025). At Lokeryggen, good agreement in the upper part of the ice column is reached, but the values diverge below 0.3 (Figure S1g). Peaks are observed at approximately 0.4 across all positions, while a second deeper peak appears near the bed at the east flank and the divide.

Fabric strength, K & C

For both ice rises, K increases more rapidly above the single maximum threshold ($\ln(K) > 0$) on the west flank and the divide than on the east flank, indicating a faster transition from isotropic material to single maximum (Figures 3a and c). Profiles from both ice rises follow similar trends, with comparable K values, suggesting broadly similar fabric types across the two structures.

Besides the fabric type K, the fabric intensity C displays a similar pattern (Figures 3e and g) for both ice rise flanks. In contrast, at the ice divide (Figure 3f), Hammarryggen exhibits significantly higher C values than Lokeryggen, pointing to a sharper single maximum fabric. This pattern is consistent with the results observed for λ_3 and $\Delta\lambda_V$, which together suggest that c-axes are more closely clustered in the vertical direction at the Hammarryggen divide than at Lokeryggen.

Vertical strain rate, $\dot{\varepsilon}_{zz}$

Figure 4 presents profiles of vertical strain rates, $\dot{\varepsilon}_{zz}$, derived from repeat pRES surveys conducted during the 2018 and 2019 field seasons. Since the resulting profiles are somewhat noisy, smoothing within discrete depth windows of the ice column (1-0.8, 0.8-0.7, 0.7-0.6, 0.6-0.5, 0.5-0.4 and 0.4-0.3) has been introduced, following Kingslake and others (2014) and Ershadi and others (2025). Near-surface values of $\dot{\varepsilon}_{zz}$ are large in magnitude (between -1.3×10^{-3} and -2.0×10^{-3} a^{-1}), reflecting rapid compaction of the shallow ice (Kingslake and others, 2014). In contrast, near the bed, $\dot{\varepsilon}_{zz}$ magnitudes are smaller, though remaining larger on the Hammarryggen flanks than at the divide, indicating slower downward motion of ice layers at the divide compared to the flanks (Figures 4a, b and c). Comparing the two Hammarryggen flanks, we observe larger magnitudes of $\dot{\varepsilon}_{zz}$ on the east flank, as we observed lower values of C and λ_3 on that same flank (Figure 2c; Figure 3g). This lowered deformation rate can suggest weaker fabric on this side of the ice rise. However, the differences between the flanks and the centre are consistent with increased ice stiffness at the divide, which limits vertical deformation and produces the upward-arching layers, or Raymond arches

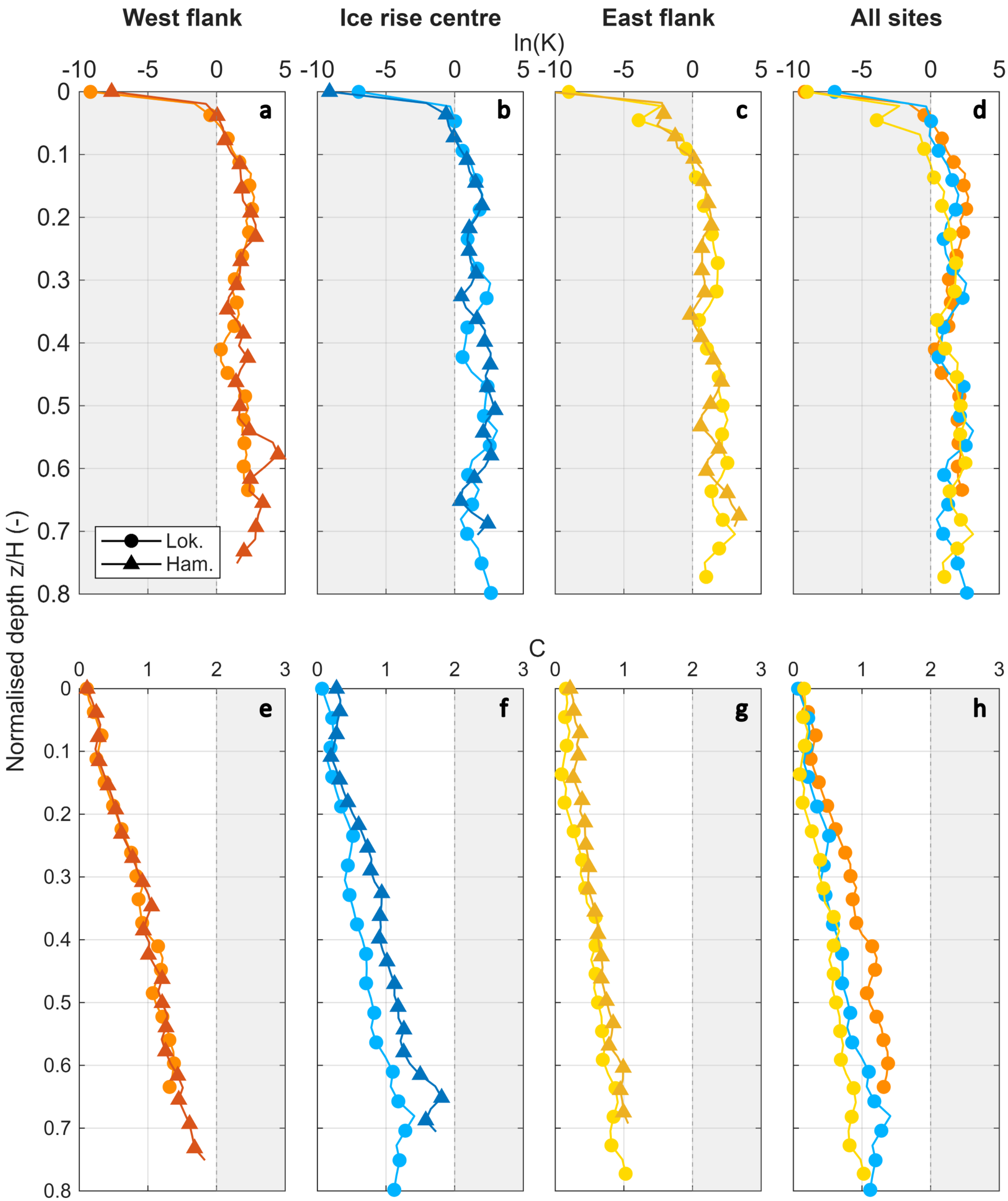

Fig. 3. Comparison of the variation of the Woodcock parameters K and C with depth at the flanks and the centre of Lokeryggen and Hammarryggen. Panels d and h display Woodcock parameters for Lokeryggen.

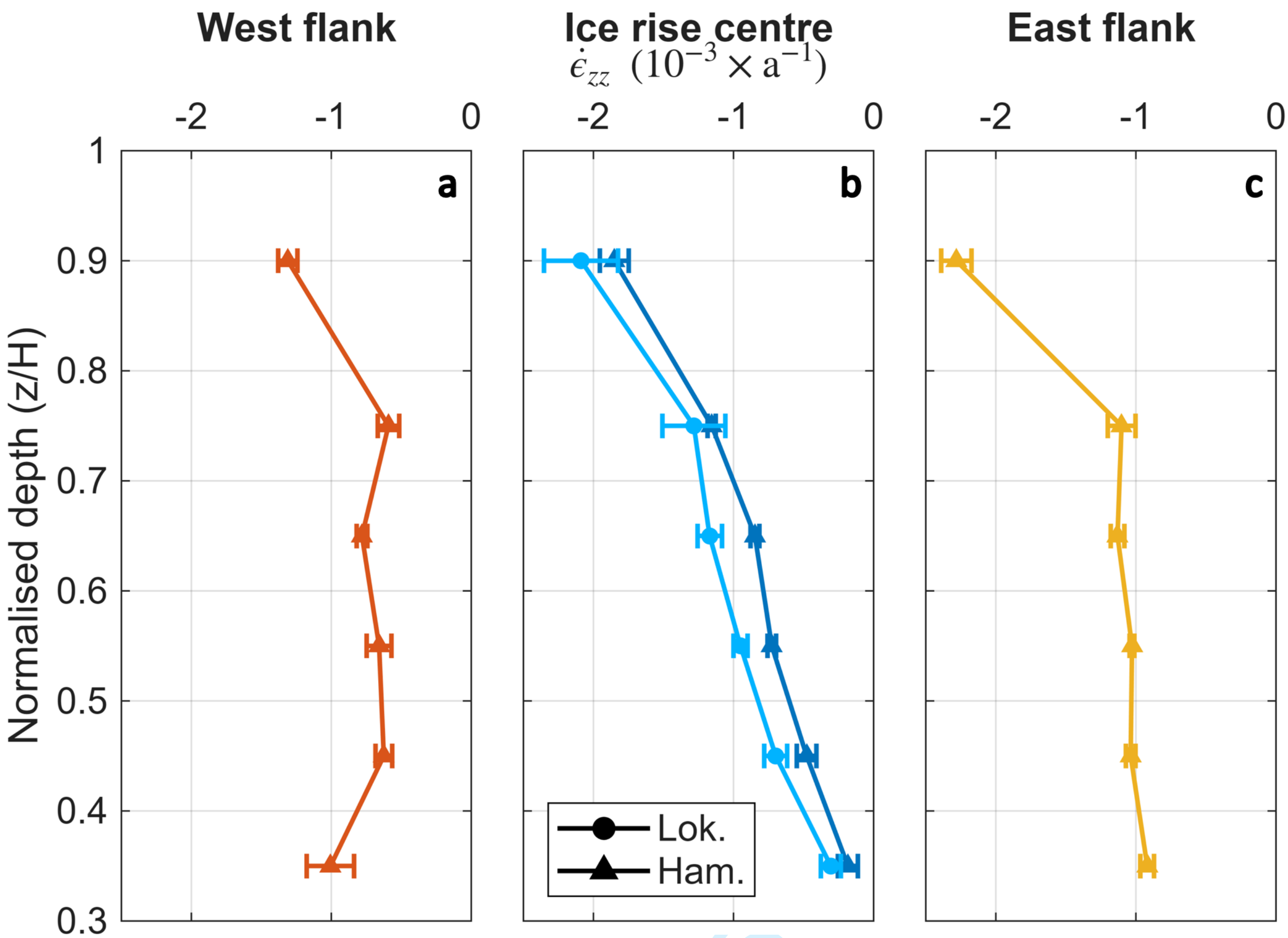

Fig. 4. Comparison of the vertical variation of the mean vertical strain rate, $\dot{\varepsilon}_{zz}$, in Hammarryggen and Lokeryggen.

(Martín and others, 2009a; Kingslake and others, 2014). For Lokeryggen, repeat measurements are only available at the divide, preventing a spatial comparison with the flanks (Gillain and others, 2026). Values of $\dot{\varepsilon}_{zz}$ at the divide follow the same pattern as observed at Hammarryggen, but are consistently larger in magnitude throughout the ice column (Figure 4b).

DISCUSSION

The rheology of these Dronning Maud Land ice rises has previously been studied. For instance, Hammarryggen has been analysed using low-frequency radio-echo sounding (Matsuoka and others, 2012; Pattyn and others, 2012), ice core fabric analysis, and phase-sensitive radar data (Pattyn and others, 2023; Koch and others, 2024; Wauthy and others, 2024; Ershadi and others, 2025). In this paper, we compare these results to pRES data from a neighbouring ice rise. Given their geographic proximity and shared classification as promontory ice rises, and a presumably similar ice dynamic history (Favier and others, 2016), we expect Hammarryggen and Lokeryggen to exhibit similar rheological characteristics. However, our results show that this is not entirely the case: while the Raymond effect is present under Hammarryggen, it seems absent at Lokeryggen.

The inverse model we used to infer the ice fabric relies on two main assumptions: (i) $\vec{v}_3$ is vertically oriented and (ii) the material at the surface is isotropic, allowing the fabric to be reconstructed in a top-to-bottom approach (Fujita and others, 2006; Ershadi and others, 2022, 2025). As explained in Ershadi and others (2025), although the first assumption can be relaxed (Rathmann and others, 2022), several factors suggest that the inverse model is applicable at both Hammarryggen and Lokeryggen. The vertical compression regime occurring in ice rises enhances c-axes to orient in the direction of the compression (Alley, 1992; Ershadi and others, 2025). Additionally, the absence of a triple junction geometry at Lokeryggen makes it potentially more suitable for such an inversion than Hammarryggen, since this type of geometry leads to complex ice flow dynamics and related fabric (Ershadi and others, 2025). Regarding the second assumption, the presence of snow at the surface likely provides a more isotropic medium than deeper ice. However, the uncertainties linked to this assumption remain unconstrained due to the absence of ice core fabric analysis at Lokeryggen. Consequently, the inverse modelling approach seems suitable for Lokeryggen, owing to its favourable geometry and compression-dominated flow regime. Therefore, the differences observed between Hammarryggen and Lokeryggen may reflect genuine rheological distinctions between the two ice rises.

At each site, the joint patterns of $\dot{\varepsilon}_{zz}$, λ_3 and $\Delta\lambda_H$ provide a multi-proxy signature of the underlying flow regime and the strengthening of the ice (Ershadi and others, 2025). At Hammarryggen, a local minimum in magnitude of $\dot{\varepsilon}_{zz}$ around 0.4-0.3 of the ice column coincides with maxima in λ_3 and $\Delta\lambda_H$ beneath the divide, Figures 5b and d. These patterns converge toward a stronger single maximum fabric at the centre of the ice rise compared to the flanks, leading to stiffer ice at the divide and the formation of anticlines (Martín and others, 2009b; Ershadi and others, 2025). The development of the Raymond effect and associated arches at Hammarryggen is confirmed by airborne radar images (Koch and others, 2024; Ershadi and others, 2025). At Lokeryggen, the vertical profile of $\dot{\varepsilon}_{zz}$ follows a similar trend to the one at Hammarryggen, although with a consistently larger magnitude. The absence of flank measurements of the downward movement of ice layers at Lokeryggen prevents a comparison between the flanks and divide values, limiting our ability to determine a spatial pattern across the transect. However, local maxima in

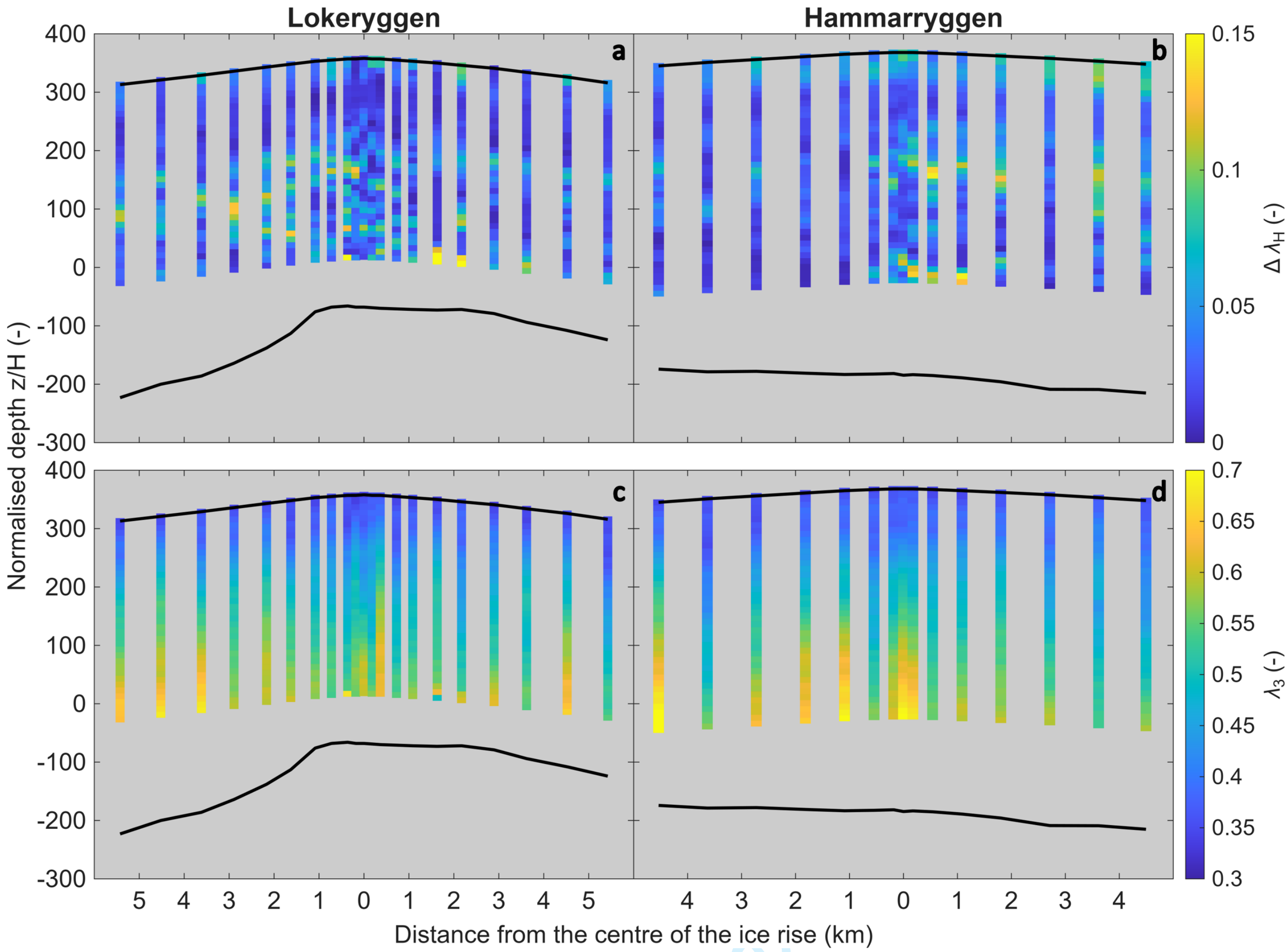

Fig. 5. Comparison of the vertical variation of $\Delta\lambda_H$ (top) and λ_3 (bottom) along the measurement transect at Lokeryggen (left) and Hammarryggen (right), together with the corresponding bedrock and surface elevations.

λ_3 and $\Delta\lambda_H$ beneath the Lokeryggen divide are absent, suggesting softer ice and the absence of Raymond arches (Figures 5a and c). Our observations are consistent with the absence of clear upward-arching ice layers at Lokeryggen (Figure S2).

The absence of a Raymond effect may arise from non-steady conditions close to the bed, which reduce ice anisotropy and resulting ice stiffening (Raymond, 1983; Nereson and others, 1998; Martín and others, 2009a; Drews and others, 2015; Matsuoka and others, 2015; Wearing and Kingslake, 2019). Another possible reason is a local migration of the divide that leads to a displacement or an asymmetry of the Raymond arches. In the case of fast or stochastic migration, arches can be totally erased (Nereson and others, 1998; Martín and others, 2009a,b). However, tilted, relict or multi-generational arch structures induced by migration are not observed (Figure S2). Instead, the internal layer architecture and surface topography closely follow the bedrock topography, without the presence of clear Raymond arches. As can be seen from

Figure 5, Hammarryggen presents a relatively flat bedrock, allowing steady-flow conditions for stiffening of the ice and formation of anticlines and amplification of their amplitude (Pettit and others, 2007). However, the summit at Lokeryggen coincides with an underlying bedrock bump (Figure 5 and Figure S2), consistent with the bedrock topography exerting a control over the internal layer architecture. Previous studies have reported such control, preventing the formation of visible arches and in others altering their amplitude and shape (Kingslake and others, 2014; Fudge and others, 2023; Goel and others, 2026). Together with the lower anisotropy and softer ice fabric inferred from pRES measurements inversion (λ_3, $\Delta\lambda_H$, $\Delta\lambda_V$, K, C and $\dot{\varepsilon}_{zz}$), the bed-surface topography coincidence supports our hypothesis that the bedrock most likely controls the expression of the Raymond effect at Lokeryggen, through its influence on ice flow dynamics. The irregular bedrock may also weaken the validity of the model first assumption, as a dynamical component may develop near the bed and cause $\vec{v}_3$ to be deviated from its assumed vertical orientation. Nevertheless, our observations are restricted to 5 (Hammarryggen) and 6 km-long (Lokeryggen) transects. Confirming the impact of uneven bedrock topography on ice fabric would require longer profiles or flow simulation using Lokeryggen bedrock geometry.

CONCLUSIONS

We analyse the rheological properties of two ice rises in Dronning Maud Land based on pRES measurements to reconstruct ice fabric and vertical strain rates. While the ice fabric is in overall agreement between the two ice rises, we observe a lower anisotropy at Lokeryggen, suggesting a lower degree of ice stiffening compared to Hammarryggen. We attribute this lower anisotropy to the effect of the bedrock, due to the alignment of internal layers underneath the Lokeryggen summit with the observed bedrock high. Apart from previously proposed explanations of ice rise age and divide migration, our analysis suggests that bedrock topography may also exert a control on the development of Raymond arches.

While inferring fabric in ice sheets is traditionally obtained using ice core analysis, the inversion of a single pRES dataset allows for the reconstruction of multiple fabric parameter profiles, demonstrating the potential of pRES as a logistically efficient and powerful tool for investigating ice rheology.

SUPPLEMENTARY MATERIAL

The supplementary material for this article can be found at link Supp Mat.

ACKNOWLEDGEMENTS

This work was supported by the Belgian Research Action through Interdisciplinary Networks (BRAIN-be) from the Belgian Science Policy Office (BELSPO) in the framework of the project "East Antarctic surface mass balance in the Anthropocene: observations and multi-scale modelling (Mass2Ant)" (contract no. BR/165/A2/Mass2Ant), as well as the BELSPO Policy 4 Science project "Melting Ice Shelves of Antarctica (MOAT)" (contract no. P4S/25/MOAT). The authors would like to thank the International Polar Foundation (IPF) for logistical support in the field. MAG benefited from a one-year doctoral scholarship from Université libre de Bruxelles (ULB).

REFERENCES

Alley RB (1992) Flow-law hypotheses for ice-sheet modeling. *Journal of Glaciology*, **38**(129), 245–256 (doi: 10.3189/S0022143000003658)

Bindschadler R, Vornberger P, Fleming A, Fox A, Mullins J, Binnie D, Paulsen SJ, Granneman B and Gorodetzky D (2008) The landsat image mosaic of antarctica. *Remote sensing of environment*, **112**(12), 4214–4226, ISSN 0034-4257 (doi: https://doi.org/10.1016/j.rse.2008.07.006)

Brisbourne AM, Martín C, Smith AM, Baird AF, Kendall JM and Kingslake J (2019) Constraining recent ice flow history at korff ice rise, west antarctica, using radar and seismic measurements of ice fabric. *Journal of Geophysical Research: Earth Surface*, **124**(1), 175–194 (doi: 10.1029/2018JF004776)

Drews R, Matsuoka K, Martín C, Callens D, Bergeot N and Pattyn F (2015) Evolution of derwael ice rise in dronning maud land, antarctica, over the last millennia. *Journal of Geophysical Research: Earth Surface*, **120**(3), 564–579 (doi: 10.1002/2014JF003246)

Ershadi MR, Drews R, Martín C, Eisen O, Ritz C, Corr H, Christmann J, Zeising O, Humbert A and Mulvaney R (2022) Polarimetric radar reveals the spatial distribution of ice fabric at domes and divides in east antarctica. *The Cryosphere*, **16**(5), 1719–1739 (doi: 10.5194/tc-16-1719-2022)

Ershadi MR, Drews R, Tison JL, Martín C, Henry ACJ, Oraschewski FM, Tsibulskaya V, Sun S, Wauthy S, Koch I and et al (2025) Investigating the dynamic history of a promontory ice rise using radar data. *Journal of Glaciology*, **71**, e1 (doi: 10.1017/jog.2024.70)

Favier L, Pattyn F, Berger S and Drews R (2016) Dynamic influence of pinning points on marine ice-sheet stability: a numerical study in dronning maud land, east antarctica. *The Cryosphere*, **10**(6), 2623–2635 (doi: 10.5194/tc-10-2623-2016)

Fudge TJ, Hills BH, Horlings AN, Holschuh N, Christian JE, Davidge L, Hoffman A, O'Connor GK, Christianson K and Steig EJ (2023) A site for deep ice coring at west hercules dome: results from ground-based geophysics and modeling. *Journal of Glaciology*, **69**(275), 538–550 (doi: 10.1017/jog.2022.80)

Fujita S, Maeno H and Matsuoka K (2006) Radio-wave depolarization and scattering within ice sheets: a matrix-based model to link radar and ice-core measurements and its application. *Journal of Glaciology*, **52**(178), 407–424 (doi: 10.3189/172756506781828548)

Gerber TA, Lilien DA, Rathmann NM, Franke S, Young TJ, Valero-Delgado F, Ershadi MR, Drews R, Zeising O, Humbert A, Stoll N, Weikusat I, Grinsted A, Hvidberg CS, Jansen D, Miller H, Helm V, Steinhage D, O'Neill C, Paden J, Gogineni SP, Dahl-Jensen D and Eisen O (2023) Crystal orientation fabric anisotropy causes directional hardening of the northeast greenland ice stream. *Nature Communications*, **14**(1), 2653, ISSN 2041-1723 (doi: 10.1038/s41467-023-38139-8)

Gillain MA, Pattyn F, Sun S and Cavitte M (2026) Polarimetric radar data collected at lokeryggen ice rise, antarctica (doi: 10.5281/zenodo.21981748)

Goel V, Martín C, Matsuoka K, Pratap B, Moholdt G, Dey R, Laluraj CM and Thamban M (2026) A new coastal ice-core site identified in dronning maud land, antarctica, for high-resolution climate reconstructions to the last glacial maximum. *The Cryosphere*, **20**(2), 1363–1378 (doi: 10.5194/tc-20-1363-2026)

Henry ACJ, Martín C and Drews R (2025) Modelling the three-dimensional, diagnostic fabric anisotropy field of an ice rise. *Journal of Glaciology*, **71**, e31 (doi: 10.1017/jog.2025.14)

Hills BH, Holschuh N, Hoffman AO, Horlings AN, Erwin E, Kirkpatrick LR, Fudge TJ, Steig EJ and Christianson K (2025a) Radar-derived crystal orientation fabric suggests dynamic stability at the summit of hercules dome. *Journal of Geophysical Research: Earth Surface*, **130**(3), e2023JF007588 (doi: https://doi.org/10.1029/2023JF007588), e2023JF007588 2023JF007588

Hills BH, Young TJ, Lilien DA, Babcock E, Bienert N, Blankenship D, Bradford J, Brighi G, Brisbourne A, Dall J, Drews R, Eisen O, Ershadi MR, Gerber TA, Holschuh N, Jansen D, Jordan TM, Karlsson NB, Li J, Martín C, Matsuoka K, May D, Oraschewski FM, Paden J, Rathmann NM, Ross N, Schroeder DM, Siegert M, Siegfried MR, Smith E and Zeising O (2025b) Radar polarimetry in glaciology: Theory, measurement techniques, and scientific applications for investigating the anisotropy of ice masses. *Reviews of Geophysics*, **63**(4), e2024RG000842 (doi: 10.1029/2024RG000842), e2024RG000842 2024RG000842

Jordan T, Schroeder D, Castelletti D, Li J and Dall J (2019) A polarimetric coherence method to determine ice crystal orientation fabric from radar sounding: Application to the neem ice core region. *IEEE Transactions on Geoscience and Remote Sensing*, **57**, 8641–8657 (doi: 10.1109/TGRS.2019.2921980)

Kingslake J, Hindmarsh RCA, Aðalgeirsdóttir G, Conway H, Corr HFJ, Gillet-Chaulet F, Martín C, King EC, Mulvaney R and Pritchard HD (2014) Full-depth englacial vertical ice sheet velocities measured using phase-sensitive radar. *Journal of Geophysical Research: Earth Surface*, **119**(12), 2604–2618 (doi: 10.1002/2014JF003275)

Koch I, Drews R, Franke S, Jansen D, Oraschewski FM, Muhle LS, Višnjević V, Matsuoka K, Pattyn F and Eisen O (2024) Radar internal reflection horizons from multisystem data reflect ice dynamic and surface accumulation history along the princess ragnhild coast, dronning maud land, east antarctica. *Journal of Glaciology*, **70**, e18 (doi: 10.1017/jog.2023.93)

Martín C, Gudmundsson GH, Pritchard HD and Gagliardini O (2009a) On the effects of anisotropic rheology on ice flow, internal structure, and the age-depth relationship at ice divides. *Journal of Geophysical Research: Earth Surface*, **114**(F4) (doi: 10.1029/2008JF001204)

Martín C, Hindmarsh RCA and Navarro FJ (2009b) On the effects of divide migration, along-ridge flow, and basal sliding on isochrones near an ice divide. *Journal of Geophysical Research: Earth Surface*, **114**(F2) (doi: https://doi.org/10.1029/2008JF001025)

Martín C, Mulvaney R, Gudmundsson GH and Corr H (2015) Inferring palaeo-accumulation records from ice-core data by an adjoint-based method: application to james ross island's ice core. *Climate of the Past*, **11**(3), 547–557 (doi: 10.5194/cp-11-547-2015)

Matsuoka K, Pattyn F, Callens D and Conway H (2012) Radar characterization of the basal interface across the grounding zone of an ice-rise promontory in east antarctica. *Annals of Glaciology*, **53**(60), 29–34 (doi: 10.3189/2012AoG60A106)

Matsuoka K, Hindmarsh RC, Moholdt G, Bentley MJ, Pritchard HD, Brown J, Conway H, Drews R, Durand G, Goldberg D, Hattermann T, Kingslake J, Lenaerts JT, Martín C, Mulvaney R, Nicholls KW, Pattyn F, Ross N, Scambos T and Whitehouse PL (2015) Antarctic ice rises and rumples: Their properties and significance for ice-sheet dynamics and evolution. *Earth-Science Reviews*, **150**, 724–745, ISSN 0012-8252 (doi: 10.1016/j.earscirev.2015.09.004)

Nereson NA, Raymond CF, Waddington ED and Jacobel RW (1998) Migration of the siple dome ice divide, west antarctica. *Journal of Glaciology*, **44**(148), 643–652 (doi: 10.3189/S0022143000002148)

Nicholls KW, Corr HF, Stewart CL, Lok LB, Brennan PV and Vaughan DG (2015) A ground-based radar for measuring vertical strain rates and time-varying basal melt rates in ice sheets and shelves. *Journal of Glaciology*, **61**(230), 1079–1087 (doi: 10.3189/2015JoG15J073)

Passchier C (1997) The fabric attractor. *Journal of Structural Geology*, **19**(1), 113–127, ISSN 0191-8141 (doi: 10.1016/S0191-8141(96)00077-6)

Pattyn F, Matsuoka K, Callens D, Conway H, Depoorter M, Docquier D, Hubbard B, Samyn D and Tison JL (2012) Melting and refreezing beneath roi baudouin ice shelf (east antarctica) inferred from radar, gps, and ice core data. *Journal of Geophysical Research: Earth Surface*, **117**(F4) (doi: https://doi.org/10.1029/2011JF002154)

Pattyn F, Wauthy S, Sun S, Tison JL and Tsibulskaya V (2023) Polarimetric radar data and ice core data collected at hammarryggen ice rise, antarctica (doi: 10.5281/zenodo.8095508)

Pettit EC and Waddington ED (2003) Ice flow at low deviatoric stress. *Journal of Glaciology*, **49**(166), 359–369 (doi: 10.3189/172756503781830584)

Pettit EC, Thorsteinsson T, Jacobson HP and Waddington ED (2007) The role of crystal fabric in flow near an ice divide. *Journal of Glaciology*, **53**(181), 277–288 (doi: 10.3189/172756507782202766)

QGIS Development Team (2026) *QGIS Geographic Information System*. QGIS Association

Rathmann NM, Lilien DA, Grinsted A, Gerber TA, Young TJ and Dahl-Jensen D (2022) On the limitations of using polarimetric radar sounding to infer the crystal orientation fabric of ice masses. *Geophysical Research Letters*, **49**(1), e2021GL096244 (doi: https://doi.org/10.1029/2021GL096244), e2021GL096244 2021GL096244

Raymond CF (1983) Deformation in the vicinity of ice divides. *Journal of Glaciology*, **29**(103), 357–373 (doi: 10.3189/S0022143000030288)

Sun S, Hattermann T, Pattyn F, Nicholls KW, Drews R and Berger S (2019) Topographic shelf waves control seasonal melting near antarctic ice shelf grounding lines. *Geophysical Research Letters*, **46**(16), 9824–9832 (doi: https://doi.org/10.1029/2019GL083881)

Wauthy S, Tison JL, Inoue M, El Amri S, Sun S, Fripiat F, Claeys P and Pattyn F (2024) Spatial and temporal variability of environmental proxies from the top 120 m of two ice cores in dronning maud land (east antarctica). *Earth System Science Data*, **16**(1), 35–58 (doi: 10.5194/essd-16-35-2024)

Wearing MG and Kingslake J (2019) Holocene formation of henry ice rise, west antarctica, inferred from ice-penetrating radar. *Journal of Geophysical Research: Earth Surface*, **124**(8), 2224–2240 (doi: 10.1029/2018JF004988)

Weikusat I, Jansen D, Binder T, Eichler J, Faria SH, Wilhelms F, Kipfstuhl S, Sheldon S, Miller H, Dahl-Jensen D and Kleiner T (2017) Physical analysis of an antarctic ice core—towards an integration of micro- and macrodynamics of polar ice. *Philosophical Transactions of the Royal Society A: Mathematical, Physical and Engineering Sciences*, **375**(2086), 20150347, ISSN 1364-503X (doi: 10.1098/rsta.2015.0347)

Woodcock NH (1977) Specification of fabric shapes using an eigenvalue method. *GSA Bulletin*, **88**(9), 1231–1236, ISSN 0016-7606 (doi: 10.1130/0016-7606(1977)88<1231:SOFSUA>2.0.CO;2)

Young TJ, Martín C, Christoffersen P, Schroeder DM, Tulaczyk SM and Dawson EJ (2021) Rapid and accurate polarimetric radar measurements of ice crystal fabric orientation at the western antarctic ice sheet (wais) divide ice core site. *The Cryosphere*, **15**(8), 4117–4133 (doi: 10.5194/tc-15-4117-2021)

Zeising O, Gerber TA, Eisen O, Ershadi MR, Stoll N, Weikusat I and Humbert A (2023) Improved estimation of the bulk ice crystal fabric asymmetry from polarimetric phase co-registration. *The Cryosphere*, **17**(3), 1097–1105 (doi: 10.5194/tc-17-1097-2023)

Topographic control on ice anisotropy in Antarctic ice rises inferred from phase-sensitive radar

Marie-Axelle GILLAIN[1]*, Carlos MARTÍN[2], Frank PATTYN[1]

[1]*Laboratoire de Glaciologie, Université libre de Bruxelles, Brussels, Belgium*

[2]*British Antarctic Survey, Natural Environment Research Council, Cambridge, UK*

Correspondence: Marie-Axelle Gillain <marie-axelle.gillain@ulb.be>

SUPPLEMENTARY MATERIAL

REFERENCES

Matsuoka K, Pattyn F, Callens D and Conway H (2012) Radar characterization of the basal interface across the grounding zone of an ice-rise promontory in east antarctica. *Annals of Glaciology*, **53**(60), 29–34 (doi: 10.3189/2012AoG60A106)

Pattyn F, Matsuoka K, Callens D, Conway H, Depoorter M, Docquier D, Hubbard B, Samyn D and Tison JL (2012) Melting and refreezing beneath roi baudouin ice shelf (east antarctica) inferred from radar, gps, and ice core data. *Journal of Geophysical Research: Earth Surface*, **117**(F4) (doi: https://doi.org/10.1029/2011JF002154)

*Present address: Laboratoire de Glaciologie, Université libre de Bruxelles, Brussels, Belgium.

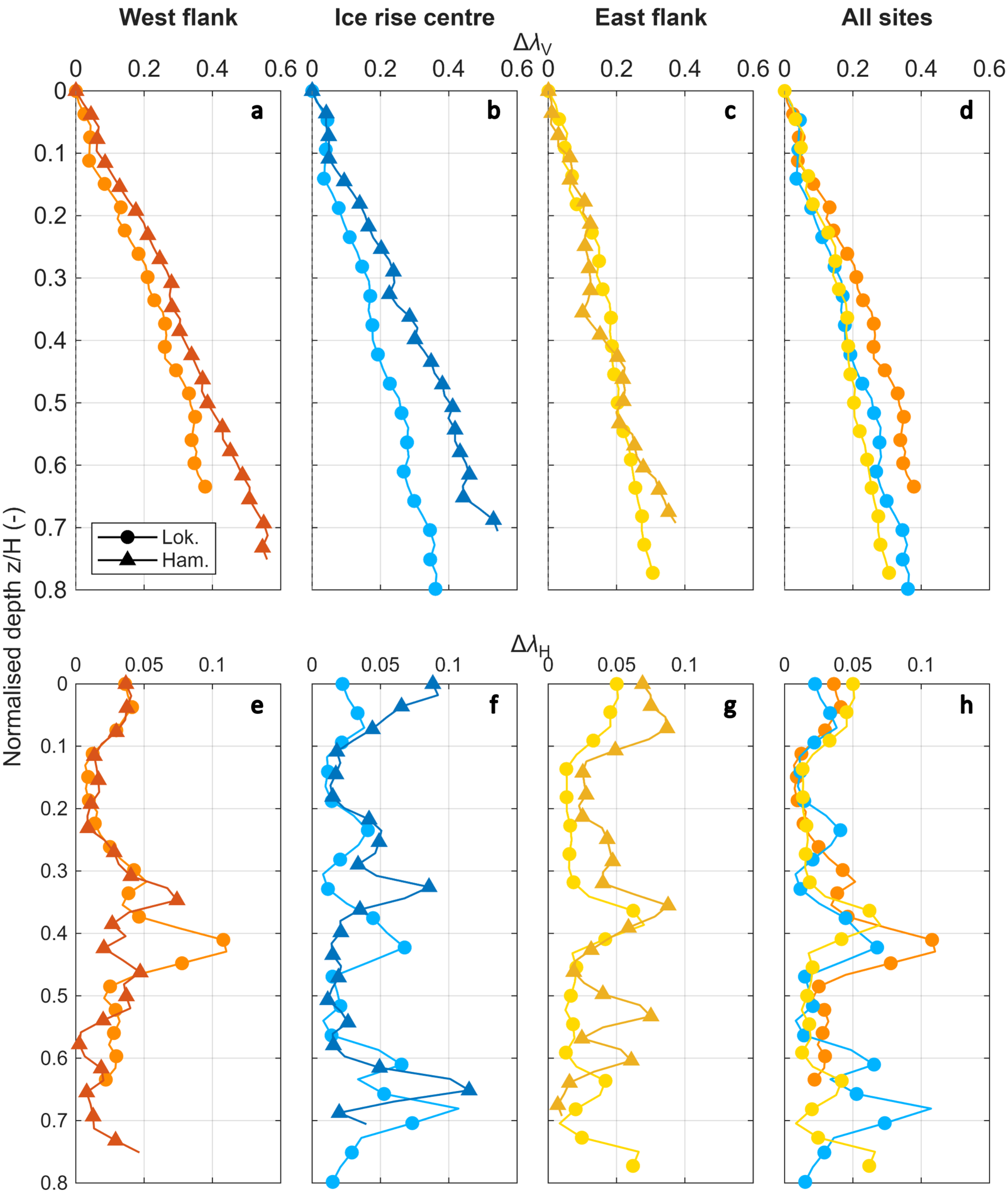

Fig. S1. Variation of $\Delta\lambda_V$ and $\Delta\lambda_H$ with depth. (a–c) Comparison of $\Delta\lambda_V$ between Lokeryggen (circles) and Hammarryggen (triangles). (d) Comparison of $\Delta\lambda_V$ between the flanks and the centre of Lokeryggen. (e–g) Comparison of $\Delta\lambda_H$ between Lokeryggen and Hammarryggen. (h) Comparison of $\Delta\lambda_H$ between the flanks and the centre of Lokeryggen.

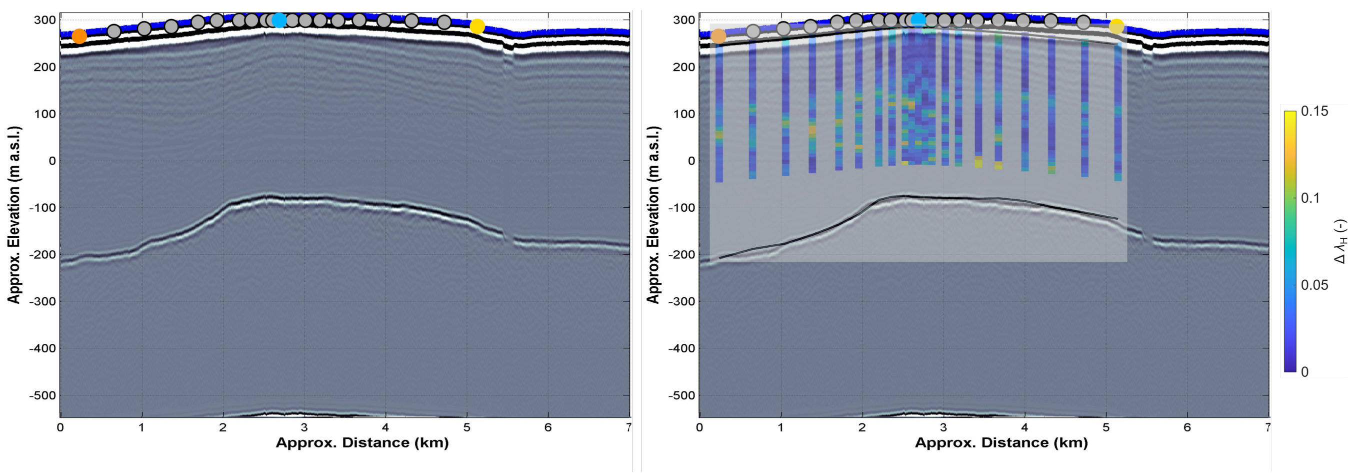

Fig. S2. Radargram across the centre of Lokeryggen, collected during the 2008-10 field seasons (Pattyn and others, 2012; Matsuoka and others, 2012). Dots indicate the pRES measurement points.